D_s-meson leading-twist distribution amplitude within the QCD sum rules and its application to the $B_s \to D_s$ transition form factor

Yi Zhang,[1,†] Tao Zhong,[2,‡] Hai-Bing Fu,[2,§] Wei Cheng,[3,∥] and Xing-Gang Wu[1,4,*]

[1]*Department of Physics, Chongqing University, Chongqing 401331, People's Republic of China*
[2]*Department of Physics, Guizhou Minzu University, Guiyang 550025, People's Republic of China*
[3]*State Key Laboratory of Theoretical Physics, Institute of Theoretical Physics, Chinese Academy of Sciences, Beijing 100190, People's Republic of China*
[4]*Chongqing Key Laboratory for Strongly Coupled Physics, Chongqing 401331, People's Republic of China*

(Received 2 April 2021; accepted 1 June 2021; published 25 June 2021)

We make a detailed study of the D_s-meson leading-twist light-cone distribution amplitude $\phi_{2;D_s}$ by using the QCD sum rules within the framework of the background field theory. To improve the precision, its moments $\langle\xi^n\rangle_{2;D_s}$ are calculated up to dimension-six condensates. At the scale $\mu = 2$ GeV, we obtain $\langle\xi^1\rangle_{2;D_s} = -0.261^{+0.020}_{-0.020}$, $\langle\xi^2\rangle_{2;D_s} = 0.184^{+0.012}_{-0.012}$, $\langle\xi^3\rangle_{2;D_s} = -0.111^{+0.007}_{-0.012}$, and $\langle\xi^4\rangle_{2;D_s} = 0.075^{+0.005}_{-0.005}$. Using those moments, the $\phi_{2;D_s}$ is then constructed by using the light-cone harmonic oscillator model. As an application, we calculate the transition form factor $f_+^{B_s\to D_s}(q^2)$ within the light-cone sum rules (LCSR) approach by using a right-handed chiral current, in which the terms involving $\phi_{2;D_s}$ dominate the LCSR. It is noted that the extrapolated $f_+^{B_s\to D_s}(q^2)$ agrees with the lattice QCD prediction. After extrapolating the transition form factor to the physically allowable q^2 region, we calculate the branching ratio and the CKM matrix element, which give $\mathcal{B}(\bar{B}_s^0 \to D_s^+\ell\nu_\ell) = (2.03^{+0.35}_{-0.49}) \times 10^{-2}$ and $|V_{cb}| = (40.00^{+4.93}_{-4.08}) \times 10^{-3}$.

DOI: 10.1103/PhysRevD.103.114024

I. INTRODUCTION

Since the first measurement of the ratio $\mathcal{R}(D^{(*)})$ of the branching fractions $\mathcal{B}(B \to D^{(*)}\tau\nu_\tau)$ and $\mathcal{B}(B \to D^{(*)}\ell\nu_\ell)$ (where ℓ stands for the light lepton e or μ) was reported by the *BABAR* Collaboration, the $B \to D^{(*)}$ semileptonic decays have attracted great attention due to large differences between the experimental measurements [1–4] and the standard model predictions [5–14]. Such differences have been considered as evidence of new physics. Comparing with the $B^{0,+}$ decays, because its background contamination from the partial reconstruction decay could be less serious, the $B_s \to D_s\ell\nu_\ell$ decay is experimentally attractive. A natural question is whether there is also evidence of new physics in the semileptonic decay $B_s \to D_s\ell\nu_\ell$. This decay could also be an important channel for determining the Cabibbo-Kobayashi-Maskawa (CKM) matrix element $|V_{\rm cb}|$.

The LHCb Collaboration reported the measurement of $|V_{\rm cb}|$ by using $B_s^0 \to D_s^-\mu^+\nu_\mu$ and $B_s^0 \to D_s^{*-}\mu^+\nu_\mu$ decays [15], in which the data of proton-proton collisions at the center-of-mass energies of 7 and 8 TeV with an integrated luminosity about 3 fb^{-1} was used in the analysis. By using the Caprini-Lellouch-Neubert (CLN) and Boyd-Grinstein-Lebed (BGL) parametrizations [16–19] for the $B_s \to D_s$ transition form factor (TFF), the determined $|V_{\rm cb}|$ are $(41.4 \pm 0.6 \pm 0.9 \pm 1.2) \times 10^{-3}$ and $(42.3 \pm 0.8 \pm 0.9 \pm 1.2) \times 10^{-3}$, respectively. The LHCb Collaboration also measured the ratio of the branching fractions $\mathcal{B}(B_s^0 \to D_s^-\mu^+\nu_\mu)$ and $\mathcal{B}(B^0 \to D^-\mu^+\nu_\mu)$, i.e., $\mathcal{R} = 1.09 \pm 0.05 \pm 0.06 \pm 0.05$, which then gives $\mathcal{B}(B_s^0 \to D_s^-\mu^+\nu_\mu) = (2.49 \pm 0.12 \pm 0.14 \pm 0.16) \times 10^{-2}$.

The accuracy of theoretical predictions on the branching fraction $\mathcal{B}(B_s \to D_s\ell\nu_\ell)$ depends heavily on the TFF $f_+^{B_s\to D_s}(q^2)$. It has been calculated within several approaches, such as the quark models [20–22], the light-front quark models [23,24], the QCD light-cone sum rules (LCSR) [25,26], and lattice QCD (LQCD) [27–29]. Similar to the $B \to \pi$ TFFs [30], the LQCD prediction is reliable in the large-q^2 region, the QCD factorization or quark model predictions are reliable in the large-recoil

*Corresponding author.
wuxg@cqu.edu.cn
†yizhangphy@cqu.edu.cn
‡zhongtao1219@sina.com
§fuhb@cqu.edu.cn
∥chengw@cqu.edu.cn

region $q^2 \sim 0$, and LCSR is reliable in the low- and intermediate-q^2 regions. Predictions under various methods are complementary to each other. Because the LCSR prediction is applicable in a wider region and could be adapted for all q^2 regions via proper extrapolations, and in this paper we adopt the LCSR approach to calculate $f_+^{B_s\to D_s}(q^2)$.

Generally, contributions from the light-cone distribution amplitude (LCDA) suffer from power-counting rules based on the twists, i.e., the high-twist LCDAs are usually powered suppressed to the lower twist ones in large-Q^2 region. The high-twist LCDAs may have sizable contributions to LCSR, and how to "design" a proper correlator is a tricky problem for the LCSR approach. By choosing a proper correlator, one can not only study the properties of the hadrons but also simplify the theoretical uncertainties effectively. As the usual treatment, the correlator is constructed by using the currents with definite quantum numbers, such as those with definite J^P, where J is the total angular momentum and P is the parity of the bound state. Such a construction of the correlator is not the only choice suggested in the literature, e.g., the chiral correlator with a chiral current in between the matrix element has also been suggested to suppress the hazy contributions from the uncertain LCDAs [31–36]. In this paper, we adopt a chiral correlator to do the LCSR calculation, and we find that the leading-twist LCDA $\phi_{2;D_s}$ provides dominant contributions. Therefore, if an accurate $\phi_{2;D_s}$ has been achieved, we shall obtain an accurate prediction of $f_+^{B_s\to D_s}(q^2)$.

Until now, there have been few calculations on the D_s-meson leading-twist LCDA $\phi_{2;D_s}$; recently, it has been studied by using the light-front quark model [37]. We first construct a light-cone harmonic oscillator model for $\phi_{2;D_s}$ based on the well-known Brodsky-Huang-Lepage (BHL) description [38–40], as we have done for π, ρ, D, and heavy meson LCDAs [41–48]. Then, its input parameters are fixed by using reasonable constraints, such as the probability of finding the leading Fock state in the D_s-meson Fock-state expansion, the normalization condition, and the calculated LCDA moments $\langle\xi^n\rangle_{2;D_s}$ or the Gegenbauer moments $a_n^{D_s}$. All of these moments are computed by using the QCD sum rules [49] within the framework of background field theory (BFT) [50] up to dimension-six operators.

The remainder of the paper is organized as follows. The LCSR for the $B_s\to D_s$ TFF, the QCD sum rules of the moments of $\phi_{2;D_s}$, and the light-cone harmonic oscillator model for $\phi_{2;D_s}$ are given in Sec. II. Numerical results and discussions are presented in Sec. III. Section IV is reserved for a summary. Useful functions for calculating the $\phi_{2;D_s}$ moments are listed in the Appendix.

II. CALCULATION TECHNOLOGY

A. LCSR for the $B_s \to D_s$ TFF

The $B_s\to D_s$ TFF $f_+^{B_s\to D_s}(q^2)$ and $\tilde{f}^{B_s\to D_s}(q^2)$ are usually defined as

$$\begin{aligned}&\langle D_s(p)|\bar{c}\gamma_\mu b|B_s(p+q)\rangle\\&\quad= 2p_\mu f_+^{B_s\to D_s}(q^2) + q_\mu \tilde{f}^{B_s\to D_s}(q^2),\end{aligned}\tag{1}$$

where p is the momentum of the D_s meson and q is the momentum transfer. In this paper, we focus on the semileptonic decay $B_s\to D_s\ell\bar{\nu}_\ell$, with $\ell=(e,\mu)$. The masses of light leptons are negligible, and due to chiral suppression only $f_+^{B_s\to D_s}(q^2)$ is relevant for our present analysis.

To derive the LCSR of $f_+^{B_s\to D_s}(q^2)$, we adopt the following chiral correlation function (correlator):

$$\begin{aligned}\Pi_\mu(p,q) &= i\int d^4x e^{ip\cdot x}\langle D_s(p)|T\{\bar{c}(x)\gamma_\mu(1+\gamma_5)b(x),\\&\qquad \bar{b}(0)i(1+\gamma_5)s(0)\}|0\rangle\\&= \Pi[q^2,(p+q)^2]p_\mu + \tilde{\Pi}[q^2,(p+q)^2]q_\mu.\end{aligned}\tag{2}$$

The correlator is analytic in whole q^2 region. In the timelike region, by inserting a complete series of the intermediate hadronic states into the correlator, one can obtain its hadronic representation by isolating the pole term of the lowest state of the B_s meson. By further using the TFF definition (1) and the B_s-meson decay constant f_{B_s},

$$\langle B_s|\bar{b}i\gamma_5 s|0\rangle = m_{B_s}^2 f_{B_s}/m_b,\tag{3}$$

where m_{B_s} is the B_s-meson mass and m_b is the b-quark mass, the hadronic representation for the correlator (2) reads

$$\begin{aligned}\Pi^{\rm had}[q^2,(p+q)^2] &= \frac{2f_+^{B_s\to D_s}(q^2)m_{B_s}^2 f_{B_s}}{m_b[m_{B_s}^2-(p+q)^2]}\\&\quad+\int_{s_0^{B_s}}^\infty \frac{\rho^{\rm QCD}(s)}{s-(p+q)^2}ds,\end{aligned}\tag{4}$$

where $s_0^{B_s}$ is a threshold parameter, $\rho^{\rm QCD}(s)$ is the spectral density, and we have implicitly used the conventional quark-hadron duality ansatz. On the other hand, in the spacelike region, the correlator can be calculated by using the operator production expansion (OPE) approach. It is done by using the b-quark propagator

$$\langle 0|Tb(x)\bar{b}(0)|0\rangle = \int\frac{d^4k}{(2\pi)^4}e^{-ik\cdot x}\frac{\not{k}+m_b}{k^2-m_b^2}+\cdots.\tag{5}$$

By matching the hadronic representation (4) and the OPE of the correlator (2) with the help of the dispersion relation, the LCSR of $f_+^{B_s\to D_s}(q^2)$ can be obtained,

$$\begin{aligned}f_+^{B_s\to D_s}(q^2) &= \frac{e^{m_{B_s}^2/M^2}}{m_{B_s}^2 f_{B_s}}\Big[F_0(q^2,M^2,s_0^{B_s})\\&\quad+\frac{\alpha_s C_F}{4\pi}F_1(q^2,M^2,s_0^{B_s})\Big],\end{aligned}\tag{6}$$

where $C_F = 4/3$, M is the Borel parameter. Here the Borel transformation has been adopted to suppress continuum contributions. The leading-order contribution of $f_+^{B_s\to D_s}(q^2)$ takes the form

$$F_0(q^2, M^2, s_0^{B_s}) = \frac{m_b^2 f_{D_s}}{m_{B_s}^2 f_{B_s}} e^{m_{B_s}^2/M^2} \int_\Delta^1 \frac{du}{u} \phi_{2;D_s}(u) \times \exp\left[-\frac{m_b^2 - \bar{u}(q^2 - u m_{D_s}^2)}{u M^2}\right], \quad (7)$$

with the D_s-meson decay constant f_{D_s} and

$$\Delta = \frac{1}{2m_{D_s}^2}\left[\sqrt{(s_0^{B_s} - q^2 - m_{D_s}^2)^2 + 4m_{D_s}^2(m_b^2 - q^2)} - (s_0^{B_s} - q^2 - m_{D_s}^2)\right].$$

The next-to-leading-order contribution of $f_+^{B_s\to D_s}(q^2)$ reads

$$F_1(q^2, M^2, s_0^{B_s}) = \frac{f_{D_s}}{\pi}\int_{m_b^2}^{s_0^{B_s}} ds e^{-s/M^2} \int_0^1 du \mathrm{Im}_s T_1(q^2, s, u)\phi_{2;D_s}(u). \quad (8)$$

The imaginary part of the next-to-leading-order amplitude T_1 can be found in Ref. [51]. Due to the present choice of the chiral correlator (2), contributions from the twist-3 D_s-meson LCDA exactly vanish in the LCSR. Thus, the terms from the omitted gluonic field in the b-quark propagator (5) and hence contributions from even higher-twist terms are negligibly small and can be safely neglected. Our remaining task is then to achieve a precise $\phi_{2;D_s}$.

B. Sum rules for the moments of the D_s-meson leading-twist LCDA $\phi_{2;D_s}$

The D_s-meson leading-twist LCDA $\phi_{2;D_s}$ is defined as

$$\langle 0|\bar{c}(z)\not{z}\gamma_5 s(-z)|D_s(q)\rangle = i(z\cdot q) f_{D_s}\int_0^1 dx e^{i(2x-1)(z\cdot q)}\phi_{2;D_s}(x), \quad (9)$$

where f_{D_s} is the D_s-meson decay constant. The moments of $\phi_{2;D_s}(x)$ can be derived by expanding the left-hand side of Eq. (9) around $z = 0$ and the exponent on the right-hand side of Eq. (9) as a power series, e.g.,

$$\langle 0|\bar{c}(0)\not{z}\gamma_5(z\cdot \overleftrightarrow{D})^n s(0)|D_s(q)\rangle = i f_{D_s}(z\cdot q)^{n+1}\langle\xi^n\rangle_{2;D_s}, \quad (10)$$

where the nth moment is defined as

$$\langle\xi^n\rangle_{2;D_s} = \int_0^1 dx(2x-1)^n\phi_{2;D_s}(x). \quad (11)$$

The zeroth moment satisfies the normalization condition

$$\langle\xi^0\rangle_{2;D_s} = 1. \quad (12)$$

The sum rules of these moments can be derived by using the following correlator:

$$\Pi_{2;D_s}^{(n,0)}(z,q) = i\int d^4x e^{iq\cdot x}\langle 0|T\{J_n(x)J_0^\dagger(0)\}|0\rangle = (z\cdot q)^{n+2} I_{2;D_s}^{(n,0)}(q^2), \quad (13)$$

where $n = (0, 1, 2, \ldots)$, and the currents

$$J_n(x) = \bar{c}(x)\not{z}\gamma_5(iz\cdot\overleftrightarrow{D})^n s(x), \quad (14)$$

$$J_0^\dagger(0) = \bar{s}(0)\not{z}\gamma_5 c(0). \quad (15)$$

By applying the OPE for the correlator (13) in the deep Euclidean region based on BFT [50], we obtain

$$\Pi_{2;D_s}^{(n,0)}(z,q) = i\int d^4x e^{iq\cdot x} \times\{-\mathrm{Tr}\langle 0|S_F^c(0,x)\not{z}\gamma_5(iz\cdot\overleftrightarrow{D})^n S_F^s(x,0)\not{z}\gamma_5|0\rangle + \mathrm{Tr}\langle 0|S_F^c(0,x)\not{z}\gamma_5(iz\cdot\overleftrightarrow{D})^n\bar{s}(0)s(x)\not{z}\gamma_5|0\rangle\} + \cdots, \quad (16)$$

where $S_F^c(0,x)$ and $S_F^s(x,0)$ are the c- and s-quark propagators in the BFT, $(iz\cdot\overleftrightarrow{D})^n$ stands for the vertex operators, and "$\cdots$" indicates even higher-order terms.

There are in total 40 Feynman diagrams for the present considered accuracy, e.g., up to dimension-six operators, the first and second terms in Eq. (16) contain 35 and 5 Feynman diagrams, respectively. Typical Feynman diagrams are shown in Figs. 1 and 2, and other diagrams can be obtained by permutation. In these two figures, the left and right big dots stand for the vertex operators $\not{z}\gamma_5(z\cdot\overleftrightarrow{D})^n$ and $\not{z}\gamma_5$ in the currents $J_n(x)$ and $J_0^\dagger(0)$, respectively; the cross symbol indicates the gluonic background field. There are also cases in which the cross symbol stands for the s-quark background field. In deriving the QCD sum rules for the moments, we need to know the propagators and vertex operators under BFT up to dimension-six operators, and tedious expressions for them can be found in Ref. [41]. Here, different from the case of the D meson, the mass effect in the denominator of the s-quark propagator cannot be ignored. However, considering that the s-quark mass is not large, we expand the s-quark propagator as a power series over m_s and keep

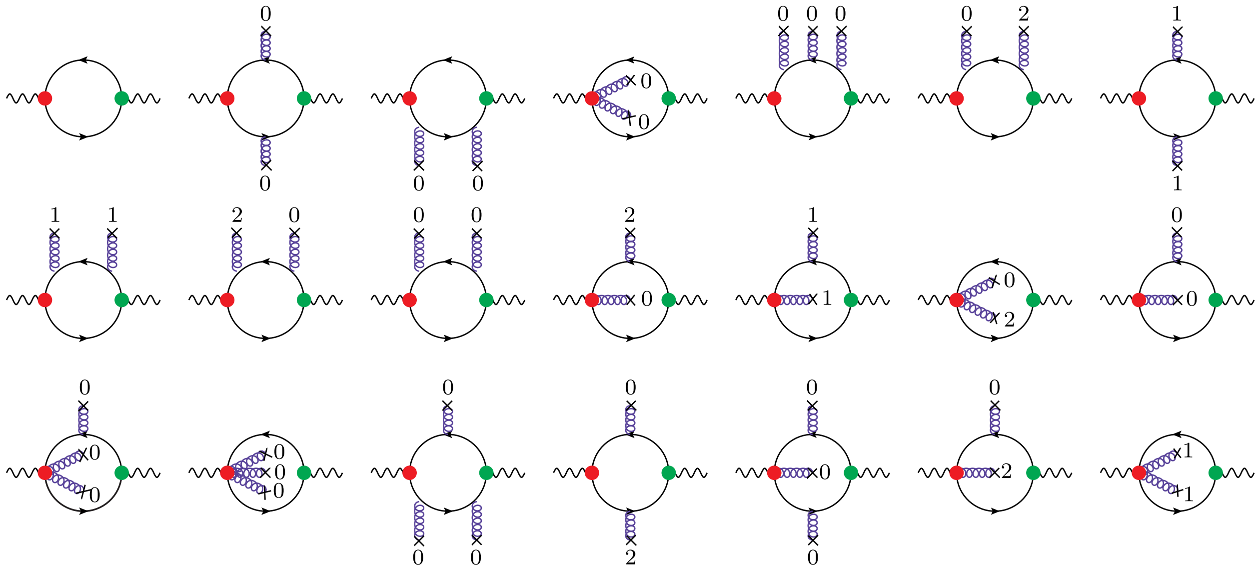

FIG. 1. Typical Feynman diagrams for the first term of Eq. (16). The left and right big dots stand for the vertex operators $\not{z}\gamma_5(z\cdot \overleftrightarrow{D})^n$ and $\not{z}\gamma_5$ in the currents $J_n(x)$ and $J_0^\dagger(0)$, respectively. The cross symbol is the gluonic background field."n" indicates the nth-order covariant derivative.

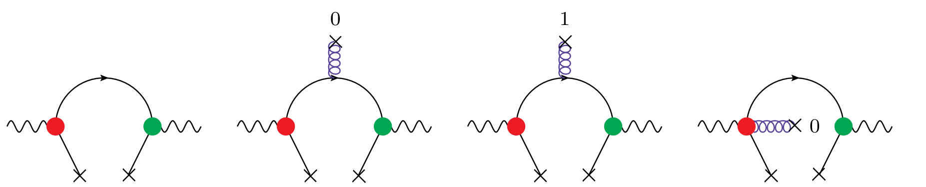

FIG. 2. Typical Feynman diagrams for the second term of Eq. (16). The left and right big dots stand for the vertex operators $\not{z}\gamma_5(z\cdot \overleftrightarrow{D})^n$ and $\not{z}\gamma_5$ in the currents $J_n(x)$ and $J_0^\dagger(0)$, respectively. The cross symbol attached to the gluon line indicates the tensor of the local gluon background field, "n" indicates the nth-order covariant derivative, and the cross symbol attached to the quark line stands for the quark background field.

only the first power of m_s. In this way, we can use the corresponding calculation technology described in detail in Ref. [44] to do the calculation.

Following the standard procedures of QCD sum rules [52,53], we obtain the sum rules for the moments of the D_s-meson leading-twist LCDA, i.e.,

$$\frac{\langle\xi^n\rangle_{2;D_s} f_{D_s}^2}{M^2} e^{-m_{D_s}^2/M^2} = \frac{1}{\pi}\frac{1}{M^2}\int_{t_{\min}}^{s_0^{D_s}} ds e^{-\frac{s}{M^2}} \mathrm{Im} I_{\rm pert}(s) + \hat{\mathcal{B}}_{M^2} I_{\langle\bar{s}s\rangle}(-q^2) + \hat{\mathcal{B}}_{M^2} I_{\langle G^2\rangle}(-q^2) + \hat{\mathcal{B}}_{M^2} I_{\langle\bar{s}Gs\rangle}(-q^2) + \hat{\mathcal{B}}_{M^2} I_{\langle\bar{s}s\rangle^2}(-q^2) + \hat{\mathcal{B}}_{M^2} I_{\langle G^3\rangle}(-q^2). \tag{17}$$

The analytical expressions of the perturbative and nonperturbative terms are

$$\begin{aligned}\mathrm{Im} I_{\rm pert}(s) = {} & \frac{3}{8\pi^2 M^2 (n+1)(n+3)}\left\{\left[\frac{1}{v}\left(1+\sqrt{1-\frac{4m_s^2 v^2}{s}}\right)-1\right]^{n+1}\left\{1-\frac{n+1}{2v}\left(1+\sqrt{1-\frac{4m_s^2 v^2}{s}}\right)\right.\right. \\ & \left.\times\left[\frac{1}{v}\left(1+\sqrt{1-\frac{4m_s^2 v^2}{s}}\right)-2\right]\right\} - \left[\frac{1}{v}\left(1-\sqrt{1-\frac{4m_s^2 v^2}{s}}\right)-1\right]^{n+1} \\ & \left.\times\left\{1-\frac{n+1}{2v}\left(1-\sqrt{1-\frac{4m_s^2 v^2}{s}}\right)\left[\frac{1}{v}\left(1-\sqrt{1-\frac{4m_s^2 v^2}{s}}\right)-2\right]\right\}\right\},\end{aligned} \tag{18}$$

$$\hat{\mathcal{B}}_{M^2} I_{2;D_s}^{\langle\bar{s}s\rangle}(-q^2) = (-1)^n e^{-m_c^2/M^2} \langle\bar{s}s\rangle \left[\frac{m_s}{M^4} + \frac{m_c^2 m_s^3}{3M^4} + \frac{(2n+1)m_s^3}{3M^6}\right], \tag{19}$$

$$\hat{\mathcal{B}}_{M^2} I_{2;D_s}^{\langle G^2\rangle}(-q^2) = \frac{\langle\alpha_s G^2\rangle}{12\pi M^4}[2n(n-1)\mathcal{H}(n-2,1,3,2) + \mathcal{H}(n,0,2,2) - 2m_c^2\mathcal{H}(n,1,1,3)], \tag{20}$$

$$\hat{\mathcal{B}}_{M^2} I_{\langle\bar{s}Gs\rangle}(-q^2) = (-1)^n e^{-m_c^2/M^2} \frac{m_s\langle g_s\bar{s}\sigma TGs\rangle}{M^6}\left[-\frac{8n+1}{18} - \frac{2m_c^2}{9M^2}\right], \tag{21}$$

$$\begin{aligned}\hat{\mathcal{B}}_{M^2} I_{\langle G^3\rangle}(-q^2) = \frac{\langle g_s^3 fG^3\rangle}{120\pi^2}&[-10(n-1)n(n+1)\mathcal{H}(n-2,1,4,3) - 30m_c^2 n(n-1)\mathcal{H}(n-2,1,4,4) - 15m_c^2 \\ &\times \mathcal{H}(n,1,1,4) - 5m_c^2\mathcal{H}(n,0,2,4) + 5nm_c^2\mathcal{H}(n-1,1,2,4) + 36m_c^4\mathcal{H}(n,1,1,5)],\end{aligned} \tag{22}$$

$$\begin{aligned}\hat{\mathcal{B}}_{M^2} I_{\langle\bar{s}s\rangle^2}(-q^2) = \frac{\langle g_s\bar{s}s\rangle^2}{2430\pi^2}&[-80n(n+1)\mathcal{H}(n-2,0,5,3) + 120m_c^2 n\mathcal{H}(n-1,0,4,4) - 60m_c^2\mathcal{H}(n,0,2,4) \\ &+ 180m_c^2\mathcal{H}(n,0,3,4) + 60(n+1)\mathcal{H}(n,0,3,3) + 25\mathcal{H}(n,0,2,3) - 80n(n+1)\mathcal{H}(n-2,2,3,3) \\ &+ 40n\mathcal{H}(n-2,1,2,3) - 120nm_c^2\mathcal{H}(n-1,1,3,4) - 50n\mathcal{H}(n-1,1,2,3) + 60nm_c^2\mathcal{H}(n-1,1,2,4) \\ &+ 120n(n-1)m_c^2\mathcal{H}(n-2,1,4,4) + 40n(n-1)(n+1)\mathcal{H}(n-2,1,4,3) - 255\mathcal{H}(n,1,1,3) \\ &+ 45m_c^2\mathcal{H}(n,1,1,4) - 144m_c^4\mathcal{H}(n,1,1,5)] \\ &+ \frac{\langle g_s\bar{s}s\rangle^2}{5832\pi^2 M^6} e^{-m_c^2/M^2}\Big\{-153[\mathcal{F}_1(n,5,3,2,\infty) - \mathcal{G}_2(n,5) + \theta(n-2)\mathcal{G}_1(n,5) + 3\theta(n-1)\mathcal{G}_2(n,5)] \\ &+ 30n\mathcal{F}_2(n-1,5,3,1,\infty) + 24n\mathcal{F}_2(n-2,5,3,1,\infty) + 2m_c m_s\mathcal{F}_2(n,4,4,1,\infty) \\ &- 18[\mathcal{F}_2(n,3,3,1,\infty) + \mathcal{G}_2(n,3)] + 15[\mathcal{F}_2(n,4,3,1,\infty) + \mathcal{G}_2(n,4)](15 + 2m_c m_s) \\ &+ \left(\ln\frac{M^2}{\mu^2} - \gamma_E + \frac{3}{2}\right)[-153(n+2)\theta(n-1) - 3)) - 30(-4\delta_{0n} - (-1)^n(2n(-1)^n\theta(n-1) + 24n \\ &+ \theta(n-2)(-1)^n - 3(-1)^n] + \left(\ln\frac{M^2}{\mu^2} - \gamma_E + \frac{11}{6}\right)[153(-1)^n + 2m_c m_s(-1)^n]\Big\},\end{aligned} \tag{23}$$

with $v = s/(s - m_c^2 + m_s^2)$. The functions $\mathcal{F}_{1,2}(n,a,b,l_{\min},l_{\max})$, $\mathcal{G}_{1,2}(n,a)$, $\mathcal{H}(n,a,b,c)$, and Borel transformations are collected in the Appendix.

C. Light-cone harmonic oscillator model for the D_s-meson leading-twist LCDA $\phi_{2;D_s}$

Based on the BHL description [38–40], similar to the case of the D-meson leading-twist LCDA [44], we construct a light-cone harmonic oscillator model of the D_s-meson leading-twist wave function $\Psi_{2;D_s}(x,\mathbf{k}_\perp)$ as

$$\Psi_{2;D_s}(x,\mathbf{k}_\perp) = \chi_{2;D_s}(x,\mathbf{k}_\perp)\Psi_{2;D_s}^R(x,\mathbf{k}_\perp), \tag{24}$$

where $\mathbf{k}_\perp$ is the transverse momentum, $\chi_{2;D_s}(x,\mathbf{k}_\perp)$ is the spin-space wave function, and $\Psi_{2;D_s}^R(x,\mathbf{k}_\perp)$ indicates the spatial wave function. The spin-space wave function $\chi_{2;D_s}(x,\mathbf{k}_\perp)$ reads [54]

$$\chi_{2;D_s}(x,\mathbf{k}_\perp) = \frac{\hat{m}_c x + \hat{m}_s(1-x)}{\sqrt{\mathbf{k}_\perp^2 + [\hat{m}_c x + \hat{m}_s(1-x)]^2}}, \tag{25}$$

where $\hat{m}_c$ and $\hat{m}_s$ are constituent quark masses of D_s, and we adopt $\hat{m}_c = 1.5$ GeV and $\hat{m}_s = 0.5$ GeV. The spatial wave function takes the form

$$\Psi_{2;D_s}^R(x,\mathbf{k}_\perp) = A_{D_s}\varphi_{2;D_s}(x) \times \exp\left[-\frac{1}{\beta_{D_s}^2}\left(\frac{\mathbf{k}_\perp^2 + \hat{m}_c^2}{1-x} + \frac{\mathbf{k}_\perp^2 + \hat{m}_s^2}{x}\right)\right], \tag{26}$$

where A_{D_s} is the normalization constant, β_{D_s} is the harmonious parameter that dominates the wave function's transverse distribution, and the function $\varphi_{2;D_s}(x)$ dominates the wave function's longitudinal distribution. $\varphi_{2;D_s}(x)$ can be taken as the first few terms of the Gegenbauer series; here, we take

$$\varphi_{2;D_s}(x) = 1 + \sum_{n=1}^{4} B_n^{D_s} C_n^{3/2}(2x-1). \tag{27}$$

By using the relationship between the D_s-meson leading-twist wave function and its LCDA at the scale μ_0,

$$\phi_{2;D_s}(x,\mu_0) = \frac{2\sqrt{6}}{f_{D_s}} \int_{|\mathbf{k}_\perp|^2 \le \mu_0^2} \frac{d^2\mathbf{k}_\perp}{16\pi^3} \Psi_{2;D_s}(x,\mathbf{k}_\perp), \tag{28}$$

which, after integrating over the transverse momentum $\mathbf{k}_\perp$, becomes

$$\begin{aligned} \phi_{2;D_s}(x,\mu_0) = {}& \frac{\sqrt{6}A_{D_s}\beta_{D_s}^2}{\pi^2 f_{D_s}} x(1-x)\varphi_{2;D_s}(x) \\ & \times \exp\left[-\frac{\hat{m}_c^2 x + \hat{m}_s^2(1-x)}{8\beta_{D_s}^2 x(1-x)}\right] \\ & \times \left\{1 - \exp\left[-\frac{\mu_0^2}{8\beta_{D_s}^2 x(1-x)}\right]\right\}, \end{aligned} \tag{29}$$

where $\mu_0 \sim \Lambda_{\rm QCD}$ is the factorization scale. Because $\hat{m}_c \gg \Lambda_{\rm QCD}$, the spin-space wave function $\chi_{D_s} \to 1$. The above model [Eqs. (24) and (29)] is for the D_s^- meson. The leading-twist wave function and the LCDA for the D_s^+ meson can be obtained by replacing x with $(1-x)$ in Eqs. (24) and (29).

The model parameters A_{D_s}, $B_n^{D_s}$, and β_{D_s} are scale dependent, their values at an initial scale μ_0 can be determined by reasonable constraints, and their values at any other scale μ can be derived via the evolution equation [55]. More explicitly, we adopt the following constraints to fix the parameters:

1. The normalization condition,

$$\int_0^1 dx \phi_{2;D_s}(x,\mu_0) = 1. \tag{30}$$

2. The probability of finding the leading Fock state $|\bar{c}s\rangle$ in the D_s-meson Fock-state expansion,

$$\begin{aligned} P_{D_s} = {}& \frac{A_{D_s}^2 \beta_{D_s}^2}{4\pi^2} x(1-x)\varphi_{D_s}^2(x) \\ & \times \exp\left[-\frac{m_c^2 x + m_s^2(1-x)}{4\beta_{D_s}^2 x(1-x)}\right]. \end{aligned} \tag{31}$$

We take $P_{D_s} \simeq 0.8$ [56] in subsequent calculations.

3. The Gegenbauer moments of $\phi_{2;D_s}(x,\mu_0)$ can be derived via the formula

$$a_n^{D_s}(\mu_0) = \frac{\int_0^1 dx \phi_{2;D_s}(x,\mu_0) C_n^{3/2}(2x-1)}{\int_0^1 dx 6x(1-x)[C_n^{3/2}(2x-1)]^2}, \tag{32}$$

and the $\phi_{2;D_s}(x,\mu_0)$ moments are defined as

$$\langle\xi^n\rangle_{2;D_s}|_{\mu_0} = \int_0^1 dx(2x-1)^n \phi_{2;D_s}(x,\mu_0). \tag{33}$$

The values of the moments $\langle\xi^n\rangle_{2;D_s}$ and the Gegenbauer moments $a_n^{D_s}$ at the scale 2 GeV are given in the next subsection.

III. NUMERICAL ANALYSIS

A. Input parameters

To do the numerical analysis of the moments of the D_s-meson leading-twist LCDA, we take the D_s-meson mass $m_{D_s} = 1.968 \pm 0.00007$ GeV, the c-quark current-quark mass $\bar{m}_c(\bar{m}_c) = 1.275 \pm 0.02$ GeV, the s-quark mass $m_s(2\ \text{GeV}) = 0.093^{+0.011}_{-0.005}$ GeV, and the decay constant of the D_s meson $f_{D_s} = 0.256 \pm 0.0042$ MeV [57]. For the gluon condensates, we take $\langle\alpha_s G^2\rangle = 0.038 \pm 0.011\ \text{GeV}^4$ and $\langle g_s^3 f G^3\rangle = 0.045\ \text{GeV}^6$ [58]. For the remaining vacuum condensates, we adopt $\langle\bar{s}s\rangle = \kappa\langle\bar{q}q\rangle$, $\langle g_s\bar{s}\sigma TGs\rangle = \kappa\langle g_s\bar{q}\sigma TGq\rangle$, and $\langle g_s\bar{s}s\rangle^2 = \kappa^2\langle g_s\bar{q}q\rangle^2$, where $\kappa = 0.74 \pm 0.03$ [59], $\langle\bar{q}q\rangle = (-2.417^{+0.227}_{-0.114}) \times 10^{-2}\text{GeV}^2$, $\langle g_s\bar{q}\sigma TGq\rangle = (-1.934^{+0.188}_{-0.103}) \times 10^{-2}\text{GeV}^5$, and $\langle g_s\bar{q}q\rangle^2 = (2.082^{+0.743}_{-0.697}) \times 10^{-3}\ \text{GeV}^6$ at $\mu = 2$ GeV [52]. The scale evolution equations of these inputs are [52,60,61]

$$\begin{aligned} \bar{m}_c(\mu) &= \bar{m}_c(\bar{m}_c)\left[\frac{\alpha_s(\mu)}{\alpha_s(\bar{m}_c)}\right]^{4/\beta_0}, \\ \bar{m}_s(\mu) &= \bar{m}_s(2\,\text{GeV})\left[\frac{\alpha_s(\mu)}{\alpha_s(2\,\text{GeV})}\right]^{4/\beta_0}, \\ \langle\bar{q}q\rangle(\mu) &= \langle\bar{q}q\rangle(2\,\text{GeV})\left[\frac{\alpha_s(\mu)}{\alpha_s(2\,\text{GeV})}\right]^{-4/\beta_0}, \\ \langle g_s\bar{q}\sigma TGq\rangle(\mu) &= \langle g_s\bar{q}\sigma TGq\rangle(2\,\text{GeV})\left[\frac{\alpha_s(\mu)}{\alpha_s(2\,\text{GeV})}\right]^{-2/(3\beta_0)}, \\ \langle g_s\bar{q}q\rangle^2(\mu) &= \langle g_s\bar{q}q\rangle^2\left[\frac{\alpha_s(\mu)}{\alpha_s(2\,\text{GeV})}\right]^{-4/\beta_0}, \\ \langle\alpha_s G^2\rangle(\mu) &= \langle\alpha_s G^2\rangle(\mu_0), \\ \langle g_s^3 f G^3\rangle(\mu) &= \langle g_s^3 f G^3\rangle(\mu_0), \end{aligned} \tag{34}$$

where $\beta_0 = 11 - 2n_f/3$, with n_f being the active quark flavors. In the following numerical calculation of the moments $\langle\xi^n\rangle_{2;D_s}|_\mu$, the scale μ will be set as the Borel parameter, as usual, i.e., $\mu = M$. The continuous threshold $s_0^{D_s}$ is usually taken as the squared mass of the D_s-meson's first excited state, and we take $s_0^{D_s} \simeq 6.5\ \text{GeV}^2$.

B. Moments $\langle\xi^n\rangle_{2;D_s}$ from QCD sum rules

To get the numerical value of the moments $\langle\xi^n\rangle_{2;D_s}$ of $\phi_{2;D_s}(x,\mu)$, one needs to fix the Borel window M^2 which is

TABLE I. Determined Borel windows and the corresponding D_s-meson leading-twist LCDA moments $\langle\xi^n\rangle_{2;D_s}$ with $n=(1,2,3,4)$. All input parameters are set to their central values. $\mu=M$.

n	M^2	$\langle\xi^n\rangle_{2;D_s}$
1	[1.517, 5.840]	[−0.304, −0.263]
2	[1.265, 4.164]	[+0.168, +0.193]
3	[2.162, 7.185]	[−0.107, −0.104]
4	[1.928, 5.524]	[+0.069, +0.077]

introduced to depress the contributions from both the continuum states and the highest-dimensional condensates. Usually, the continuum contribution and the dimension-six condensate contribution are taken to be less than 30% and 10%, respectively, while the value of $\langle\xi^n\rangle_{2;D_s}$ is required to be as stable as possible in the allowed Borel window. In this paper, the continuum state contribution for $\langle\xi^n\rangle_{2;D_s}|_\mu$ with $n=(1,2,3,4)$ is required to be less than 20%, 25%, 10%, and 30%, respectively, and each of the dimension-six condensate contributions is no more than 1%. The determined Borel windows and the corresponding D_s-meson leading-twist LCDA moments $\langle\xi^n\rangle_{2;D_s}$ at the scale $\mu=2$ GeV with $n=(1,\ldots,4)$ are presented in Table I, where all input parameters are taken set to their central values. We present the D_s-meson leading-twist LCDA moments $\langle\xi^n\rangle_{2;D_s}$ with $n=(1,\ldots,4)$ at $\mu=2$ GeV versus M^2 in Fig. 3. To be consistent with Table I, these moments are stable over the allowable Borel windows.

If we set $\mu=2$ GeV, by taking all uncertainty sources into consideration, we obtain

$$\langle\xi^1\rangle_{2;D_s}|_{\mu=2\ \mathrm{GeV}} = -0.261^{+0.020}_{-0.020}, \tag{35}$$

$$\langle\xi^2\rangle_{2;D_s}|_{\mu=2\ \mathrm{GeV}} = +0.184^{+0.012}_{-0.012}, \tag{36}$$

$$\langle\xi^3\rangle_{2;D_s}|_{\mu=2\ \mathrm{GeV}} = -0.111^{+0.007}_{-0.012}, \tag{37}$$

$$\langle\xi^4\rangle_{2;D_s}|_{\mu=2\ \mathrm{GeV}} = +0.075^{+0.005}_{-0.005}, \tag{38}$$

where the errors are squared averages of all of the mentioned error sources.

C. Determination of the model parameters of $\phi_{2;D_s}$

According to the constraints of the D_s-meson leading-twist LCDA $\phi_{2;D_s}(x,\mu)$, i.e., Eqs. (30)–(32), we need to know the Gegenbauer moments $a_n^{D_s}(\mu)$ to fix the parameters A_{D_s}, $B_n^{D_s}$, and β_{D_s}. The Gegenbauer moments $a_n^{D_s}(\mu)$, using their relations to the LCDA moments $\langle\xi^n\rangle_{2;D_s}|_\mu$ [42], are

$$a_1^{D_s}(2\ \mathrm{GeV}) = -0.436^{+0.033}_{-0.033}, \tag{39}$$

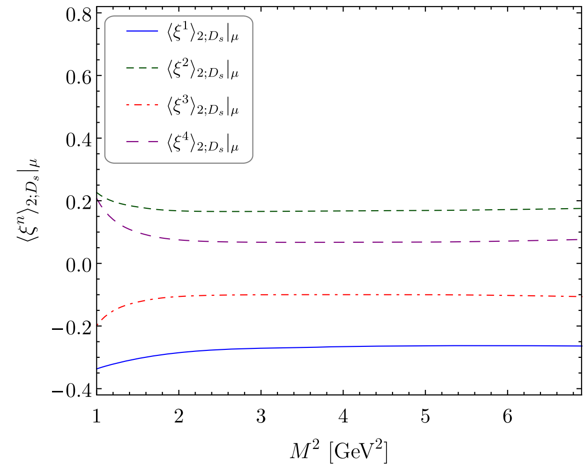

FIG. 3. D_s-meson leading-twist LCDA moments $\langle\xi^n\rangle_{2;D_s}$ at the scale $\mu=M$ with $n=(1,\ldots,4)$ versus the Borel parameter M^2, where all input parameters are set to their central values.

$$a_2^{D_s}(2\ \mathrm{GeV}) = -0.047^{+0.035}_{-0.035}, \tag{40}$$

$$a_3^{D_s}(2\ \mathrm{GeV}) = +0.004^{+0.010}_{-0.020}, \tag{41}$$

$$a_4^{D_s}(2\ \mathrm{GeV}) = -0.004^{+0.025}_{-0.026}, \tag{42}$$

We present all of the determined input parameters at the scale $\mu=2$ GeV in Table II. The accuracy of $\phi_{2;D_s}(x,\mu)$ is dominated by the magnitudes of the Gegenbauer moments $a_n^{D_s}(\mu)$. As we have pointed out in Refs. [44,45], the Gegenbauer moments $a_n^{D_s}(\mu)$ are correlated to each other and cannot be changed independently within their own error regions. Then, Table II associates the uncertainty of $\phi_{2;D_s}(x,\mu)$ with the error of the Gegenbauer moments $a_n^{D_s}(\mu)$, which facilitates our further discussion on the impact of $\phi_{2;D_s}(x,\mu)$ as an input parameter to the $B_s\to D_s$ decay.

Figure 4 shows the D_s-meson leading-twist LCDA $\phi_{2;D_s}(x,\mu)$ with typical values of the input parameters listed in Table II. The solid, dash-dotted, and dashed lines are for the parameters listed in the second, third, and forth lines of Table II. Our model of $\phi_{2;D_s}(x,\mu)$ prefers a broader behavior in the low-x region. It has a peak around $x\sim0.35$. Figure 5 shows the D_s-meson leading-twist LCDA $\phi_{2;D_s}(x,\mu)$ at different scales, where the solid, dashed, dotted, and dash-dotted lines are for the scales $\mu=2$, 3, 10, 100 GeV, respectively. It shows that with the increment of μ, $\phi_{2;D_s}(x,\mu)$ becomes broader and broader and becomes more symmetric, e.g., the peak moves closer to $x=0.5$. When $\mu\to\infty$, $\phi_{2;D_s}(x,\mu)$ tends to the known asymptotic form, i.e., $\phi_{2;D_s}(x,\mu\to\infty)=6x(1-x)$.

TABLE II. Typical D_s-meson leading-twist LCDA model parameters at the scale $\mu = 2$ GeV. The first line contains the central value, and the second/third line contains the upper/lower limit for the LCDA.

	$a_1^{D_s}(\mu)$	$a_2^{D_s}(\mu)$	$a_3^{D_s}(\mu)$	$a_4^{D_s}(\mu)$	$A_{D_s}(\mathrm{GeV}^{-1})$	$B_1^{D_s}$	$B_2^{D_s}$	$B_3^{D_s}$	$B_4^{D_s}$	$\beta_{D_s}(\mathrm{GeV})$
Central value	−0.436	−0.047	0.004	−0.004	2.760	−0.313	−0.185	0.083	0.008	4.521
Upper	$-0.436^{+0.033}$	$-0.047_{-0.035}$	$0.004^{+0.010}$	$-0.004_{-0.026}$	2.802	−0.290	−0.198	0.079	0.001	4.484
Lower	$-0.436_{-0.033}$	$-0.047^{+0.035}$	$0.004_{-0.020}$	$-0.004^{+0.025}$	2.717	−0.334	−0.173	0.081	0.014	4.567

D. Numerical results for the $B_s \to D_s$ TFF and its applications

Our inputs for the $B_s \to D_s$ TFF $f_+^{B_s \to D_s}(q^2)$ are [57]

$$m_{\bar{B}_s^0} = 5.36688 \pm 0.00017\ \mathrm{GeV},$$
$$\bar{m}_b(\bar{m}_b) = 4.18^{+0.04}_{-0.03}\ \mathrm{GeV},$$
$$f_{B_s} = 266 \pm 19\ \mathrm{MeV}.$$

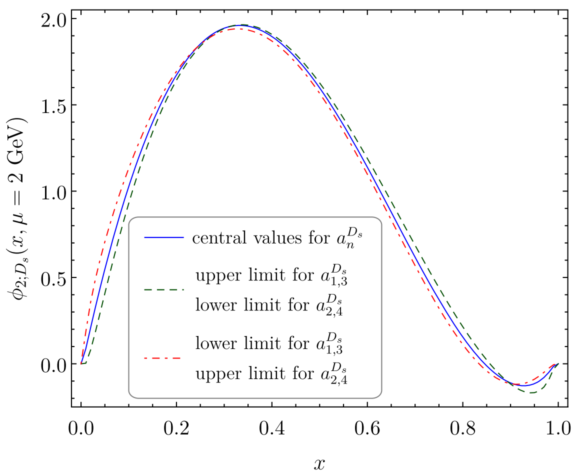

FIG. 4. D_s-meson leading-twist LCDA $\phi_{2;D_s}(x, \mu)$ with the parameter values listed in Table II.

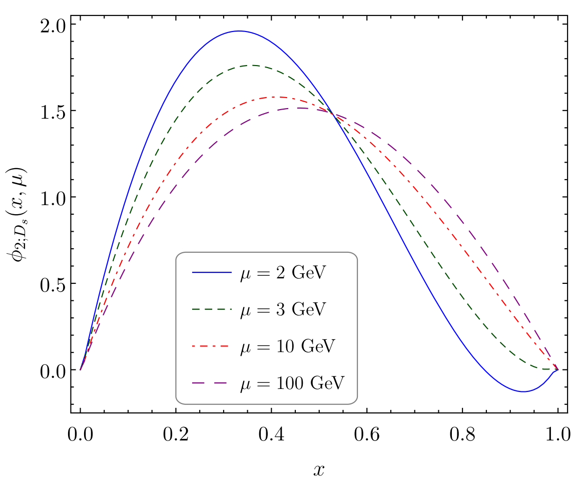

FIG. 5. D_s-meson leading-twist LCDA $\phi_{2;D_s}(x, \mu)$ at different scales, where the solid, dashed, dotted and dash-dotted lines are for $\mu = 2$, 3, 10, 100 GeV, respectively.

There are still two parameters to be fixed: the continuum threshold $s_0^{B_s}$ and the Borel window M^2. We set $s_0^{B_s} = 38 \pm 1\ \mathrm{GeV}^2$ and $M^2 = (20\text{–}30)\ \mathrm{GeV}^2$ with the scale $\mu \simeq 3$ GeV, which is close to $\sqrt{m_{B_s}^2 - m_b^2}$. Such a choice makes the TFF $f_+^{B_s \to D_s}(q^2)$ stable within the allowable Borel window, as can be seen in Fig. 6. At the large-recoil point $q^2 = 0$, we obtain

$$f_+^{B \to D}(0) = 0.639^{+0.056}_{-0.009}|_{\phi_{2;D_s}}{}^{+0.005}_{-0.013}|_{M^2}{}^{+0.014}_{-0.015}|_{s_0^{B_s}} {}^{+0.043}_{-0.049}|_{f_{B_s}} \pm 0.010|_{f_{D_s}}{}^{+0.018}_{-0.012}|_{m_b}, \quad (43)$$

and in the zero-recoil region $q^2 = q^2_{\max}$, we obtain

$$f_+^{B \to D}(q^2_{\max}) = 1.189 \pm 0.125, \quad (44)$$

where all of the uncertainties have been added in quadrature, and the errors from $\phi_{2;D_s}(x, \mu)$ and f_{B_s} dominate the uncertainties. It agrees with the lattice QCD predictions within errors: $f_+^{B_s \to D_s}(0) = 0.656(31)$ [28] and $f_+^{B_s \to D_s}(0) = 0.666(12)$ [29].

Figure 6 also shows that for larger q^2 values, the TFF will show a sizable dependence on M^2, which agrees with the convention that the LCSR approach cannot be applied for very large q^2 values. We adopt the TFF $f_+^{B_s \to D_s}(q^2)$ within the region $[0, 9\ \mathrm{GeV}^2]$ as a basis to extrapolate it to

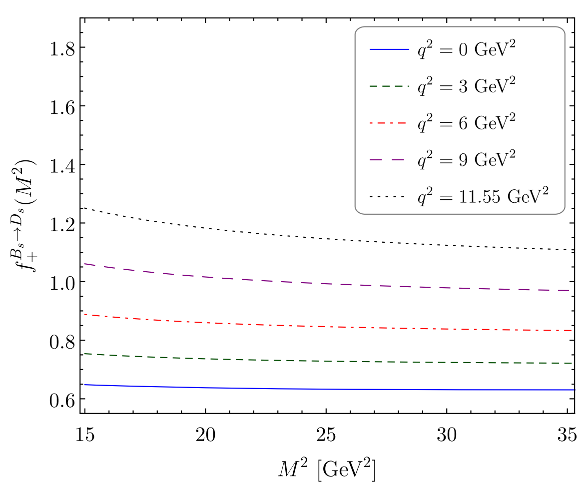

FIG. 6. TFF $f_+^{B_s \to D_s}(q^2)$ for some typical q^2 values versus the Borel parameter M^2.

TABLE III. Parameters a and b for the TFF extrapolation. The lowest, middle, and highest TFFs are adopted for such a determination.

$f_+^{B_s\to D_s}(0)$	a	b
0.639	1.350	0.479
0.583	1.345	0.531
0.714	1.320	0.443

all physical q^2 values. For this purpose, we adopt the double-pole-extrapolation method [62] to do the extrapolation, i.e.,

$$f_+^{B_s\to D_s}(q^2) = \frac{f_+^{B_s\to D_s}(0)}{1 - a(q^2/m_{B_s}^2) + b(q^2/m_{B_s}^2)^2}. \tag{45}$$

The fitted parameters are listed in Table III.

The extrapolated results are presented in Fig. 7, where the solid line is the central value of $f_+^{B_s\to D_s}(q^2)$ and the lighter shaded band shows its theoretical uncertainty, in which the uncertainties from all of the mentioned error sources, such as $\phi_{2;D_s}(x,\mu)$, $s_0^{B_s}$, f_{B_s}, f_{D_s}, m_b, etc., have been added in quadrature. As a comparison, the lattice QCD predictions for the large-q^2 points and its extrapolation to the entire q^2 region have are also shown, and the thicker shaded band represents the errors [28]. Our results agree well with the lattice QCD predictions, especially the arising trends over the changes of q^2 are close to each other.

As applications, we adopt the LCSR prediction for the TFF to make a prediction of the CKM matrix element $|V_{cb}|$ and the branching ratio $\mathcal{B}(B_s \to D_s \ell \bar\nu_\ell)$.

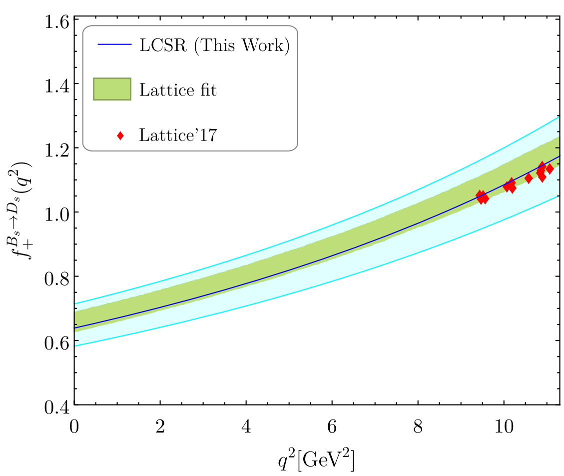

FIG. 7. Extrapolated LCSR prediction for the TFF $f_+^{B_s\to D_s}(q^2)$, where the lighter shaded band is the squared average from all of the mentioned error sources. The lattice QCD prediction and its extrapolated results given in 2017 [28] are also presented as a comparison, and the thicker shaded band shows its uncertainty.

The TFF at the zero-recoil point, $f_+^{B_s\to D_s}(q^2_{\rm max})$, is often quoted as

$$\mathcal{G}(1) = \frac{2\sqrt{m_{B_s} m_{D_s}}}{m_{B_s} + m_{D_s}} \times f_+^{B_s\to D_s}(q^2_{\rm max}). \tag{46}$$

Using the averaged value given by the *BABAR* Collaboration via the measurements on the semileptonic decay $\bar B \to D\ell\bar\nu_\ell$ [63,64], $\eta_{\rm ew}\mathcal{G}(1)|V_{cb}| = (42.65 \pm 1.53)\times 10^{-3}$, we obtain $|V_{cb}| = (40.003^{+4.929}_{-4.075})\times 10^{-3}$. In Table IV we present a comparison of $|V_{cb}|$ with the LHCb measured values under the CLN and BGL approaches [15], the HPQCD prediction [12], the Particle Data Group (PDG) averaged value [57], the *BABAR* measured value [65], the BELLE measured values under the CLN + LQCD and BGL + LQCD approaches [66], and the lattice QCD prediction [67].

We adopt the extrapolated TFF $f_+^{B_s\to D_s}(q^2)$ to calculate the branching ratio $\mathcal{B}(B_s \to D_s\ell\bar\nu_\ell)$, which can be derived by using the following formula:

$$\mathcal{B}(B_s \to D_s\ell\bar\nu_\ell) = \tau_{B_s}\int_0^{(m_{B_s}-m_{D_s})^2} dq^2 \frac{d\Gamma(B_s \to D_s\ell\bar\nu_\ell)}{dq^2}, \tag{47}$$

where the differential decay width is

$$\frac{d\Gamma(B_s \to D_s\ell\bar\nu_\ell)}{dq^2} = \frac{G_F^2|V_{\rm cb}|^2}{192\pi^3 m_{B_s}^3}\lambda^{3/2}(q^2)|f_+^{B_s\to D_s}(q^2)|^2, \tag{48}$$

where $G_F = 1.1663787(6)\times 10^{-5}$ GeV^{-2} and the phase-space factor $\lambda(q^2) = (m_{B_s}^2 + m_{D_s}^2 - q^2)^2 - 4m_{B_s}^2 m_{D_s}^2$. We present the differential decay width $1/|V_{cb}|^2 \times d\Gamma/dq^2$ in Fig. 8. After considering the B_s-meson lifetime $\tau_{B_s} = (1.510 \pm 0.004)\times 10^{-12}$ s [57], we obtain

$$\mathcal{B}(\bar B_s^0 \to D_s^+\ell\nu_\ell) = (2.033^{+0.350}_{-0.488})\times 10^{-2}. \tag{49}$$

TABLE IV. Comparison of $|V_{cb}|$ under various approaches and the experimentally measured values.

References	$\lvert V_{cb}\rvert \times 10^{-3}$
This work	$40.003^{+4.929}_{-4.075}$
LHCb (CLN) [15]	$41.4 \pm 0.6 \pm 0.9 \pm 1.2$
LHCb (BGL) [15]	$42.3 \pm 0.8 \pm 0.9 \pm 1.2$
HPQCD [12]	$39.6 \pm 1.7 \pm 0.2$
PDG [57]	41.0 ± 1.4
BABAR [65]	38.36 ± 0.9
BELLE (CLN + LQCD) [66]	$38.4 \pm 0.2 \pm 0.6 \pm 0.6$
BELLE (BGL + LQCD) [66]	$38.3 \pm 0.3 \pm 0.7 \pm 0.6$
LQCD [67]	41.3 ± 2.2

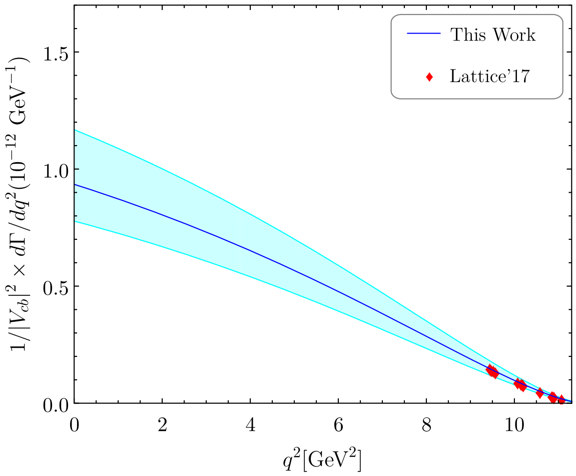

FIG. 8. Differential decay width $1/|V_{cb}|^2 \times d\Gamma/dq^2$, with $\ell = (e, \mu)$. As a comparison, we also present the lattice QCD predictions at the large-q^2 points [28].

IV. SUMMARY

In this work, we have made a detailed study of the D_s-meson leading-twist LCDA $\phi_{2;D_s}$. Its moments have been calculated using the QCD sum rules within the framework of BFT, and its first four moments have been given in Eqs. (35)–(38), which then result in the Gegenbauer moments $a_1^{D_s}(2\ \mathrm{GeV}) = -0.436^{+0.033}_{-0.033}$, $a_2^{D_s}(2\ \mathrm{GeV}) = -0.047^{+0.035}_{-0.035}$, $a_3^{D_s}(2\,\mathrm{GeV}) = 0.004^{+0.01}_{-0.02}$, and $a_4^{D_s}(2\ \mathrm{GeV}) = -0.004^{-0.026}_{+0.025}$. Based on the BHL prescription, we have constructed a new model for $\phi_{2;D_s}$, whose behavior is constrained by the normalization condition, the probability of finding the leading Fock state $|\bar{c}s\rangle$ in the D_s-meson Fock-state expansion, and the known Gegenbauer moments. As the key input for studying the high-energy processes involving the D_s meson, our suggested $\phi_{2;D_s}$ will be of great importance.

Using the present model of $\phi_{2;D_s}$, we calculated the $B_s \to D_s$ TFF $f_+^{B_s\to D_s}(q^2)$ within the QCD LCSR approach by adopting a chiral current correlator, in which the leading-twist terms dominant over the LCSR. In the large-recoil region, we obtained $f_+^{B_s\to D_s}(0) = 0.639^{+0.075}_{-0.056}$. By using the extrapolated TFF with the double-pole-extrapolation method, we obtained $\mathcal{B}(\bar{B}_s^0 \to D_s{}^+\ell\nu_\ell) = (2.033^{+0.350}_{-0.488}) \times 10^{-2}$ and the CKM element $|V_{cb}| = (40.00^{+4.929}_{-4.075}) \times 10^{-3}$, which is consistent with the various measurements within reasonable errors.

ACKNOWLEDGMENTS

This work was supported in part by the National Natural Science Foundation of China under Grants No. 11625520, No. 11765007, No. 11947406, and No. 12047564, the Graduate Research and Innovation Foundation of Chongqing, China (Grant No. ydstd1912), the Project of Guizhou Provincial Department of Science and Technology under Grant No. KY[2019]1171, the Project of Guizhou Provincial Department of Education under Grants No. KY[2021]030 and No. KY[2021]003, the China Postdoctoral Science Foundation under Grants No. 2019TQ0329, No. 2020M670476, the Chongqing Graduate Research and Innovation Foundation under Grant No. 2020CQJQY-Z003, and the Project of Guizhou Minzu University under Grant No. GZMU[2019]YB19.

APPENDIX: USEFUL FUNCTIONS FOR CALCULATING THE MOMENTS OF $\phi_{2;D_s}$

The functions $\mathcal{F}_{1,2}(n, a, b, l_{\min}, l_{\max})$, $\mathcal{G}_{1,2}(n, a)$, and $\mathcal{H}(n, a, b, c)$ used in the sum rules (18)–(23) are

$$\mathcal{F}_1(n, a, b, l_{\min}, l_{\max}) = \sum_{k=0}^{n} \frac{(-1)^k n! \Gamma(k+a)}{k!(n-k)!} \sum_{l=l_{\min}}^{l_{\max}} \frac{\Gamma(l+b)\Gamma(n-1-k+l)}{\Gamma(n-1+l+a)} \times \sum_{i=0}^{l} \frac{1}{i!(l-i)!(l-1-i+b)!} \left(-\frac{m_c^2}{M^2}\right)^{l-i}, \tag{A1}$$

$$\mathcal{F}_2(n, a, b, l_{\min}, l_{\max}) = \sum_{k=0}^{n} \frac{(-1)^k n! \Gamma(k+a)}{k!(n-k)!} \sum_{l=l_{\min}}^{l_{\max}} \frac{\Gamma(l+b)\Gamma(n-k+l)}{\Gamma(n+l+a)} \sum_{i=0}^{l} \frac{1}{i!(l-i)!(l-1-i+b)!} \left(-\frac{m_c^2}{M^2}\right)^{l-i}, \tag{A2}$$

$$\mathcal{G}_1(n, a) = \sum_{k=0}^{n-2} \frac{(-1)^k n! \Gamma(k+a)\Gamma(n-1-k)}{k!(n-k)!\Gamma(n-1+a)}, \tag{A3}$$

$$\mathcal{G}_2(n, a) = \sum_{k=0}^{n-1} \frac{(-1)^k n! \Gamma(k+a)\Gamma(n-k)}{k!(n-k)!\Gamma(n+a)}, \tag{A4}$$

$$\mathcal{H}(n,a,b,c) = \int_0^1 dx(2x-1)^n x^a (1-x)^b \exp\left[-\frac{m_c^2}{M^2(1-x)}\right]$$
$$= \frac{1}{(c-1)!}\frac{1}{(M^2)^c}\int_0^1 dx(2x-1)^n x^a(1-x)^b \exp\left[-\frac{m_c^2}{M^2(1-x)}\right]. \quad \text{(A5)}$$

The Borel transformation formulas are

$$\hat{\mathcal{B}}_{M^2}\frac{1}{(-q^2+m_c^2)^k}\ln\frac{-q^2+m_c^2}{\mu^2} = \frac{1}{(k-1)!}\frac{1}{M^{2k}}e^{-m_c^2/M^2}\left[\ln\frac{M^2}{\mu^2}+\psi(k)\right] \quad (k\geq 1),$$
$$\hat{\mathcal{B}}_{M^2}(-q^2+m_c^2)^k\ln\frac{-q^2+m_c^2}{\mu^2} = (-1)^{k+1}k!M^{2k}e^{-m_c^2/M^2} \quad (k\geq 0),$$
$$\hat{\mathcal{B}}_{M^2}\frac{(-q^2)^l}{(-q^2+m_c^2)^{l+\tau}} = \begin{cases} 0, & \tau=0, l=0; \\ \sum_{i=0}^{l-1}\frac{l!}{i!(l-i)!(l-i-1)!}\left(-\frac{m_c^2}{M^2}\right)^{l-i}e^{-m_c^2/M^2}, & \tau=0, l>0; \\ \sum_{i=0}^{l}\frac{l!}{i!(l-i)!(l+\tau-i-1)!}\left(-\frac{m_c^2}{M^2}\right)^{l-i}\frac{1}{M^{2\tau}}e^{-m_c^2/M^2}, & \tau>0, l\geq 0. \end{cases} \quad \text{(A6)}$$

[1] J. P. Lees *et al.* (*BABAR* Collaboration), Evidence for an Excess of $\bar{B}\to D^{(*)}\tau^-\bar{\nu}_\tau$ Decays, Phys. Rev. Lett. **109**, 101802 (2012).

[2] J. P. Lees *et al.* (*BABAR* Collaboration), Measurement of an excess of $\bar{B}\to D^{(*)}\tau^-\bar{\nu}_\tau$ decays and implications for charged Higgs bosons, Phys. Rev. D **88**, 072012 (2013).

[3] M. Huschle *et al.* (Belle Collaboration), Measurement of the branching ratio of $\bar{B}\to D^{(*)}\tau^-\bar{\nu}_\tau$ relative to $\bar{B}\to D^{(*)}\ell^-\bar{\nu}_\ell$ decays with hadronic tagging at Belle, Phys. Rev. D **92**, 072014 (2015).

[4] Y. Amhis *et al.* (Heavy Flavor Averaging Group (HFAG)), Averages of b-hadron, c-hadron, and τ-lepton properties as of summer 2014, arXiv:1412.7515.

[5] F. Zuo, Z. H. Li, and T. Huang, Form factor for $B\to Dl\tilde{\nu}$ in light-cone sum rules with chiral current correlator, Phys. Lett. B **641**, 177 (2006).

[6] F. Zuo and T. Huang, $B_c(B)\to D\ell\tilde{\nu}$ form-factors in light-cone sum rules and the D meson distribution amplitude, Chin. Phys. Lett. **24**, 61 (2007).

[7] S. Fajfer, J. F. Kamenik, and I. Nisandzic, On the $B\to D^*\tau\bar{\nu}_\tau$ sensitivity to new physics, Phys. Rev. D **85**, 094025 (2012).

[8] H. B. Fu, X. G. Wu, H. Y. Han, Y. Ma, and T. Zhong, $|V_{cb}|$ from the semileptonic decay $B\to D\ell\bar{\nu}_\ell$ and the properties of the D meson distribution amplitude, Nucl. Phys. **B884**, 172 (2014).

[9] Y. Y. Fan, W. F. Wang, S. Cheng, and Z. J. Xiao, Semi-leptonic decays $B\to D^{(*)}\ell\nu$ in the perturbative QCD factorization approach, Chin. Sci. Bull. **59**, 125 (2014).

[10] Y. Y. Fan, Z. J. Xiao, R. M. Wang, and B. Z. Li, The $B\to D^{(*)}\ell\nu_\ell$ decays in the pQCD approach with the lattice QCD input, Sci. Bull. **60**, 2009 (2015).

[11] J. A. Bailey *et al.* (MILC Collaboration), $B\to D\ell\nu$ form factors at nonzero recoil and $|V_{cb}|$ from 2 + 1-flavor lattice QCD, Phys. Rev. D **92**, 034506 (2015).

[12] H. Na, C. M. Bouchard, G. P. Lepage, C. Monahan, and J. Shigemitsu (HPQCD Collaboration), $B\to D\ell\nu$ form factors at nonzero recoil and extraction of $|V_{cb}|$, Phys. Rev. D **92**, 054510 (2015).

[13] Y. M. Wang, Y. B. Wei, Y. L. Shen, and C. D. Lü, Perturbative corrections to $B\to D$ form factors in QCD, J. High Energy Phys. 06 (2017) 062.

[14] T. Zhong, Y. Zhang, X. G. Wu, H. B. Fu, and T. Huang, The ratio $\mathcal{R}(D)$ and the D-meson distribution amplitude, Eur. Phys. J. C **78**, 937 (2018).

[15] R. Aaij *et al.* (LHCb Collaboration), Measurement of $|V_{cb}|$ with $B_s^0\to D_s^{(*)-}\mu^+\nu_\mu$ decays, Phys. Rev. D **101**, 072004 (2020).

[16] I. Caprini, L. Lellouch, and M. Neubert, Dispersive bounds on the shape of $\bar{B}\to D^{(*)}\ell\bar{\nu}$ form-factors, Nucl. Phys. **B530**, 153 (1998).

[17] C. G. Boyd, B. Grinstein, and R. F. Lebed, Constraints on Form-Factors for Exclusive Semileptonic Heavy to Light Meson Decays, Phys. Rev. Lett. **74**, 4603 (1995).

[18] C. G. Boyd, B. Grinstein, and R. F. Lebed, Model independent determinations of $\bar{B}\to D\ell\bar{\nu}, D^*\ell\bar{\nu}$ form-factors, Nucl. Phys. **B461**, 493 (1996).

[19] C. G. Boyd, B. Grinstein, and R. F. Lebed, Precision corrections to dispersive bounds on form-factors, Phys. Rev. D **56**, 6895 (1997).

[20] R. N. Faustov and V. O. Galkin, Weak decays of B_s mesons to D_s mesons in the relativistic quark model, Phys. Rev. D **87**, 034033 (2013).

[21] G. Kramer and W. F. Palmer, Decay of B_s mesons into vector mesons, Phys. Rev. D **46**, 3197 (1992).

[22] X. J. Chen, H. F. Fu, C. S. Kim, and G. L. Wang, Estimating form factors of $B_s \to D_s^{(*)}$ and their applications to semi-leptonic and non-leptonic decays, J. Phys. G **39**, 045002 (2012).

[23] X. W. Kang, T. Luo, Y. Zhang, L. Y. Dai, and C. Wang, Semileptonic B and B_s decays involving scalar and axial-vector mesons, Eur. Phys. J. C **78**, 909 (2018).

[24] L. Zhang, X. W. Kang, X. H. Guo, L. Y. Dai, T. Luo, and C. Wang, A comprehensive study on the semileptonic decay of heavy flavor mesons, J. High Energy Phys. 02 (2021) 179.

[25] P. Blasi, P. Colangelo, G. Nardulli, and N. Paver, Phenomenology of B_s decays, Phys. Rev. D **49**, 238 (1994).

[26] R. H. Li, C. D. Lü, and Y. M. Wang, Exclusive B_s decays to the charmed mesons $D_s^+(1968, 2317)$ in the standard model, Phys. Rev. D **80**, 014005 (2009).

[27] M. Atoui, V. Morénas, D. Bečirevic, and F. Sanfilippo, $B_s \to D_s \ell \nu_\ell$ near zero recoil in and beyond the Standard Model, Eur. Phys. J. C **74**, 2861 (2014).

[28] C. J. Monahan, H. Na, C. M. Bouchard, G. P. Lepage, and J. Shigemitsu, $B_s \to D_s \ell \nu$ form factors and the fragmentation fraction ratio f_s/f_d, Phys. Rev. D **95**, 114506 (2017).

[29] E. McLean, C. T. H. Davies, J. Koponen, and A. T. Lytle, $B_s \to D_s \ell \nu$ Form factors for the full q^2 range from Lattice QCD with non-perturbatively normalized currents, Phys. Rev. D **101**, 074513 (2020).

[30] T. Huang and X. G. Wu, Consistent calculation of the B to pi transition form-factor in the whole physical region, Phys. Rev. D **71**, 034018 (2005).

[31] T. Huang and Z. H. Li, $B \to K^*$ gamma in the light cone QCD sum rule, Phys. Rev. D **57**, 1993 (1998).

[32] T. Huang, Z. H. Li, and X. Y. Wu, Improved approach to the heavy to light form-factors in the light cone QCD sum rules, Phys. Rev. D **63**, 094001 (2001).

[33] Z. G. Wang, M. Z. Zhou, and T. Huang, $B\pi$ weak form-factor with chiral current in the light cone sum rules, Phys. Rev. D **67**, 094006 (2003).

[34] F. Zuo, Z. H. Li, and T. Huang, Form factor for $B \to Dl\nu$ in light-cone sum rules with chiral current correlator, Phys. Lett. B **641**, 177 (2006).

[35] X. G. Wu, T. Huang, and Z. Y. Fang, SU(f)(3)-symmetry breaking effects of the $B \to K$ transition form-factor in the QCD light-cone sum rules, Phys. Rev. D **77**, 074001 (2008).

[36] X. G. Wu and T. Huang, Radiative corrections on the $B \to P$ form factors with chiral current in the light-cone sum rules, Phys. Rev. D **79**, 034013 (2009).

[37] N. Dhiman, H. Dahiya, C. R. Ji, and H. M. Choi, Twist-2 pseudoscalar and vector meson distribution amplitudes in light-front quark model with exponential-type confining potential, Phys. Rev. D **100**, 014026 (2019).

[38] S. J. Brodsky, T. Huang, and G. P. Lepage, in *Particles and Fields-2*, Proceedings of the Banff Summer Institute, Banff; Alberta, 1981, edited by A. Z. Capri and A. N. Kamal (Plenum, New York, 1983), p. 143.

[39] G. P. Lepage, S. J. Brodsky, T. Huang, and P. B. Mackenize, in *Particles and Fields-2*, Proceedings of the Banff Summer Institute, Banff; Alberta, 1981, edited by A. Z. Capri and A. N. Kamal (Plenum, New York, 1983), p. 83.

[40] T. Huang, in *Proceedings ofXXth International Conference on High Energy Physics*, Madison, Wisconsin, 1980, edited by L. Durand and L. G. Pondrom, *AIP Conf. Proc.* No. 69 (AIP, New York, 1981), p. 1000.

[41] T. Zhong, X. G. Wu, Z. G. Wang, T. Huang, H. B. Fu, and H. Y. Han, Revisiting the pion leading-twist distribution amplitude within the QCD background field theory, Phys. Rev. D **90**, 016004 (2014).

[42] T. Zhong, X. G. Wu, and T. Huang, Heavy pseudoscalar leading-twist distribution amplitudes within QCD theory in background fields, Eur. Phys. J. C **75**, 45 (2015).

[43] T. Zhong, X. G. Wu, T. Huang, and H. B. Fu, Heavy pseudoscalar twist-3 distribution amplitudes within QCD theory in background fields, Eur. Phys. J. C **76**, 509 (2016).

[44] Y. Zhang, T. Zhong, X. G. Wu, K. Li, H. B. Fu, and T. Huang, Uncertainties of the $B \to D$ transition form factor from the D-meson leading-twist distribution amplitude, Eur. Phys. J. C **78**, 76 (2018).

[45] T. Zhong, Y. Zhang, X. G. Wu, H. B. Fu, and T. Huang, The ratio $\mathcal{R}(D)$ and the D-meson distribution amplitude, Eur. Phys. J. C **78**, 937 (2018).

[46] H. B. Fu, X. G. Wu, H. Y. Han, Y. Ma, and H. Y. Bi, The ρ-meson longitudinal leading-twist distribution amplitude, Phys. Lett. B **738**, 228 (2014).

[47] H. B. Fu, X. G. Wu, H. Y. Han, and Y. Ma, $B \to \rho$ transition form factors and the ρ-meson transverse leading-twist distribution amplitude, J. Phys. G **42**, 055002 (2015).

[48] L. Zeng, H. B. Fu, D. D. Hu, L. L. Chen, W. Cheng, and X. G. Wu, Revisiting the production of $J/\psi + \eta_c$ via the e^+e^- annihilation within the QCD light-cone sum rules, Phys. Rev. D **103**, 056012 (2021).

[49] M. A. Shifman, A. I. Vainshtein, and V. I. Zakharov, QCD and resonance physics. Theoretical foundations, Nucl. Phys. **B147**, 385 (1979).

[50] T. Huang and Z. Huang, Quantum chromodynamics in background fields, Phys. Rev. D **39**, 1213 (1989).

[51] G. Duplancic, A. Khodjamirian, T. Mannel, B. Melic, and N. Offen, Light-cone sum rules for $B \to \pi$ form factors revisited, J. High Energy Phys. 04 (2008) 014. The s-quark mass is small in comparison to the b-quark mass, so we neglect the s-quark mass effects in deriving the $B_s \to D_s$ TFF. Then the imaginary part of the NLO amplitude T_1 is the same as that of $B \to \pi$ TFF.

[52] T. Zhong, Z. H. Zhu, H. B. Fu, X. G. Wu, and T. Huang, An improved light-cone harmonic oscillator model for the pionic leading-twist distribution amplitudes, arXiv:2102.03989.

[53] D. D. Hu, H. B. Fu, T. Zhong, L. Zeng, W. Cheng, and X. G. Wu, η-meson leading-twist distribution amplitude within QCD sum rule approach and its application to the semi-leptonic decay $D_s^+ \to \eta \ell^+ \nu_\ell$, arXiv:2102.05293.

[54] T. Huang, B. Q. Ma, and Q. X. Shen, Analysis of the pion wave function in light cone formalism, Phys. Rev. D **49**, 1490 (1994).

[55] G. P. Lepage and S. J. Brodsky, Exclusive processes in perturbative quantum chromodynamics, Phys. Rev. D **22**, 2157 (1980).

[56] X. H. Guo and T. Huang, Hadronic wave functions in D and B decays, Phys. Rev. D **43**, 2931 (1991).

[57] P. A. Zyla *et al.* (Particle Data Group), Review of particle physics, Prog. Theor. Exp. Phys. **2020**, 083C01 (2020).

[58] P. Colangelo and A. Khodjamirian, QCD sum rules, a modern perspective, in *At the Frontier of Particle Physics*, edited by M. Shifman (World Scientific, Singapore, 2001), Vol. 3, pp. 1495–1576, https://doi.org/10.1142/9789812810458_0033.

[59] S. Narison, Mini-review on QCD spectral sum rules, Nucl. Part. Phys. Proc. **258–259**, 189 (2015).

[60] K. C. Yang, W. Y. P. Hwang, E. M. Henley, and L. S. Kisslinger, QCD sum rules and neutron proton mass difference, Phys. Rev. D **47**, 3001 (1993).

[61] W. Y. P. Hwang and K. C. Yang, QCD sum rules: $\Delta - N$ and $\Sigma_0 - \Lambda$ mass splittings, Phys. Rev. D **49**, 460 (1994).

[62] W. Wang, Y. L. Shen, and C. D. Lü, Covariant light-front approach for $B_{(c)}$ transition form factors, Phys. Rev. D **79**, 054012 (2009).

[63] B. Aubert *et al.* (*BABAR* Collaboration), Measurements of the semileptonic decays $\bar{B} \to D\ell\bar{\nu}$ and $\bar{B} \to D^*\ell\bar{\nu}$ using a global fit to $DX\ell\bar{\nu}$ final states, Phys. Rev. D **79**, 012002 (2009).

[64] B. Aubert *et al.* (*BABAR* Collaboration), Measurement of $|V_{cb}|$ and the Form-Factor Slope in $\bar{B} \to D\ell\nu_\ell$ Decays in Events Tagged by a Fully Reconstructed B Meson, Phys. Rev. Lett. **104**, 011802 (2010).

[65] J. P. Lees *et al.* (*BABAR* Collaboration), Extraction of form Factors from a Four-Dimensional Angular Analysis of $\bar{B} \to D^*\ell^-\bar{\nu}_\ell$, Phys. Rev. Lett. **123**, 091801 (2019).

[66] E. Waheed *et al.* (Belle Collaboration), Measurement of the CKM matrix element $|V_{cb}|$ from $B^0 \to D^{*-}\ell^+\nu_\ell$ at Belle, Phys. Rev. D **100**, 052007 (2019).

[67] J. Harrison, C. T. H. Davies, and M. Wingate (HPQCD Collaboration), Lattice QCD calculation of the $B_{(s)} \to D^*_{(s)}\ell\nu$ form factors at zero recoil and implications for $|V_{cb}|$, Phys. Rev. D **97**, 054502 (2018).